AIAA 2013-4424

Analysis of Excess Wake Vortex Separation on Arrival Delay

Kevin E. Witzberger[1] and John E. Robinson, III[2]
NASA Ames Research Center, Moffett Field, CA 94035

An analysis is performed to estimate the delay in the terminal area due to excess leading/trailing aircraft wake vortex spacing. This analysis makes use of a large database of recorded traffic from early 2010 at several of the busiest Terminal Radar Approach Control Facilities (TRACONs) in the United States. To facilitate delay estimates, two arrival compression models are developed and applied to the recorded arrival traffic. A key feature of the compression modeling is the use of just two discrete points in the trajectory: TRACON entry and runway threshold crossing, eliminating the need for the resource intensive procedure of trajectory reconstruction. The analysis has two parts and each part focuses on two runways that are dedicated entirely to arrivals: KATL 27L and KDEN 35R. The first part is a sensitivity study exploring two strategies for compressing the arrivals: path reduction with original average true airspeeds and path reduction with (often times) faster average true airspeeds. This sensitivity study results in a range of delay savings on the order of tens of seconds per flight. The rest of the analysis uses the path compression model (original average true airspeeds), showing the uneven variation of daily delay savings at KATL 27L. Cumulative distribution functions capture the excess spacing reductions. They show a 10% increase (relative to the observed excess spacing) in arrivals landing with an excess spacing of 0.5 nmi or less at KATL 27L and a 25% increase at KDEN 35R.

Nomenclature

i	=	aircraft index
$R^P_{\min}(i)$	=	statistical minimum of path distance, nmi
$\bar{V}^{\max}_{TAS}(i)$	=	statistical maximum of average true airspeed, knots
$S_R(i)$	=	minimum required leading/trailing wake vortex spacing, nmi
$R^P(i)$	=	path distance, nmi
$S^{new}(i)$	=	new leading/trailing wake vortex spacing, nmi
$S_E(i)$	=	excess spacing at runway threshold, nmi
$S_B(i)$	=	spacing buffer, nmi
$S(i)$	=	observed leading/trailing wake vortex spacing at runway threshold, nmi
$\Delta T_D(i)$	=	delay time saved, sec
$\Delta R^P(i)$	=	path distance saved, nmi
$T_{entry}(i)$	=	TRACON entry time, Unix time
$T_{runway}(i)$	=	runway threshold crossing time, Unix time
$T_D(i)$	=	estimated delay time, sec
$\Delta T^P(i)$	=	delay savings due to path compression, sec
$\Delta T^S(i)$	=	delay savings due speed compression, sec

[1] Aerospace Engineer, Aerospace High Density Operations Branch, Mail Stop 210-6, AIAA Senior Member.
[2] Chief Engineer, Aerospace Technology Demonstration #1, Mail Stop 210-6, AIAA Senior Member.

I. Introduction

A recent comprehensive study of aircraft arrivals at several of the busiest airports in the United States showed excess leading/trailing aircraft wake vortex spacing.[1] This excess spacing is an inefficiency in the terminal area that causes increased delay and fuel consumption and it degrades throughput. Due to the projection that air traffic is expected to grow 90% over the next twenty years as measured by revenue passenger miles,[2] this growth will certainly lead to more airport arrival operations that will amplify this excess spacing inefficiency. The Next Generation Air Transportation System (NextGen) is our Nation's solution for safely and efficiently handling this substantial increase in air traffic demand relative to current day operations.[3] NextGen technologies are expected to reduce this excess spacing; therefore, reducing delay, fuel consumption and increasing throughput.

Two approaches to assess the effectiveness of NextGen technologies are human-in-the-loop (HITL) simulations and statistical models. HITL simulations require supporting infrastructure (laboratory), participants, and a sufficient financial budget. Additionally, HITL simulations take significant time to organize and execute; however, they sometimes are the credible way to validate a new technology. In contrast, some assessments are more appropriately studied by statistical models. The technical tradeoff is the operational realism offered by a HITL simulation versus the faster, broader assessments enabled by statistical models. These two approaches can complement each other. For example, if a statistical model of a NextGen technology shows some potential benefits, the next step may be to access it with a HITL simulation. Data from HITL simulations can also be used to improve the statistical models. Spacing improvements have been measured/simulated using both approaches.[1, 4-6] Delay and throughput benefits have been determined based upon those results, which are specific to an airport, airport configuration, fleet mix, etc.

Recently, two studies that make use of the statistical modeling approach have quantified the potential benefits from certain NextGen technologies such as precision scheduling, sequencing, and spacing and continuous descent operations (CDO). [1,7] Both of these comprehensive studies made use of the same very large dataset of recorded traffic from 2010 (approximately 500,000 arrival flights). In Ref. 7, Robinson and Kamgarpour showed that the potential fuel savings from CDO during congested arrival periods is highly variable – day-to-day, aircraft to aircraft, etc. In Ref. 1, Zelinski analyzed the observed excess in-trail spacing for aircraft operating in instrument meteorological conditions (IMC) and visual meteorological conditions (VMC) to 29 runways in eight of the busiest Terminal Radar Approach Control Facilities (TRACONs). Zelinski assessed two major benefits of precision scheduling and spacing: (1) potential throughput increases and (2) potential flight time savings. The potential increase in throughput was determined using a separation buffer of 0.3 nmi. Performance-based navigation (PBN) such as Area Navigation (RNAV)/Required Navigation (RNP)[8] routes were modeled for each runway to assess delay savings. Flights were re-sequenced according to their new arrival times along these routes using the same speed profiles flown along the original routes. The delay savings for flights operating in VMC and IMC were estimated based on these original and new arrival times. The resource intensive procedure of trajectory reconstruction and subsequent examination to determine suitable RNAV routes was a key requirement of Zelinski's precision scheduling and spacing analysis.[9] No alternative statistical method for assessing the potential benefits of precision scheduling and spacing automation tools on excess spacing can be found in the literature.

In this study, we offer a statistical modeling method, like those discussed in Ref. 1 and Ref. 7., for assessing the potential benefits of terminal scheduling and spacing automation tools that does not require all of the complexities associated with HITL simulations. Moreover, the method presented in this paper does not require the complexity of reconstructing/generating trajectories to determine suitable RNAV routes. Our model estimates delay reduction when excess spacing is recovered by shortening each aircraft's path and (optionally) increasing its speed closer to its shortest and fastest reasonable limits, respectively. We refer to each model used to shorten the path and (optionally) increase the speed as the "traffic compression" model or "compression" model for short. This study is motivated by a desire to estimate flight time in the terminal area due to excess spacing at the runway threshold given a large arrival traffic sample (>1,000 flights) without requiring resource intensive trajectory reconstruction and examination procedures of each aircraft's route flown from the meter fix to the runway threshold. The study described in this paper quantifies potential delay savings, but is not motivated by a specific technology (e.g., RNP). NextGen technologies, however, are expected to result in more efficient terminal area operations—realizing at least some of the potential savings. Our statistical model can be viewed as a first order analysis that estimates delay savings due to reduced excess spacing. This work differs from Ref. 1 in four key ways. First, it does not require establishing RNAV/RNP routes through reconstruction of each aircraft's trajectory. In fact, the methodology used in this analysis uses trajectory states at just two key discrete points along the aircraft's arrival trajectory: entry into the TRACON and at the runway threshold. Second, the impact of speed variations, in addition to path variations, is explored. Third, the flights are segregated by meteorological condition before delay savings is estimated, whereas Ref. 1

segregates the results after delay savings is estimated. Fourth, the minimum separation requirement of 2.5 nmi is used instead of 3 nmi.[10,11]

The methodology and traffic compression models used for the analyses are discussed in detail in Section II. Section III presents the results of the delay savings analysis. Lastly, we outline our conclusions regarding the statistical traffic compression model described in this paper in Section IV.

II. Methodology

This analysis uses the recorded tracks of approximately 500,000 flights in eight different TRACONs. These flights occurred during January through May 2010.

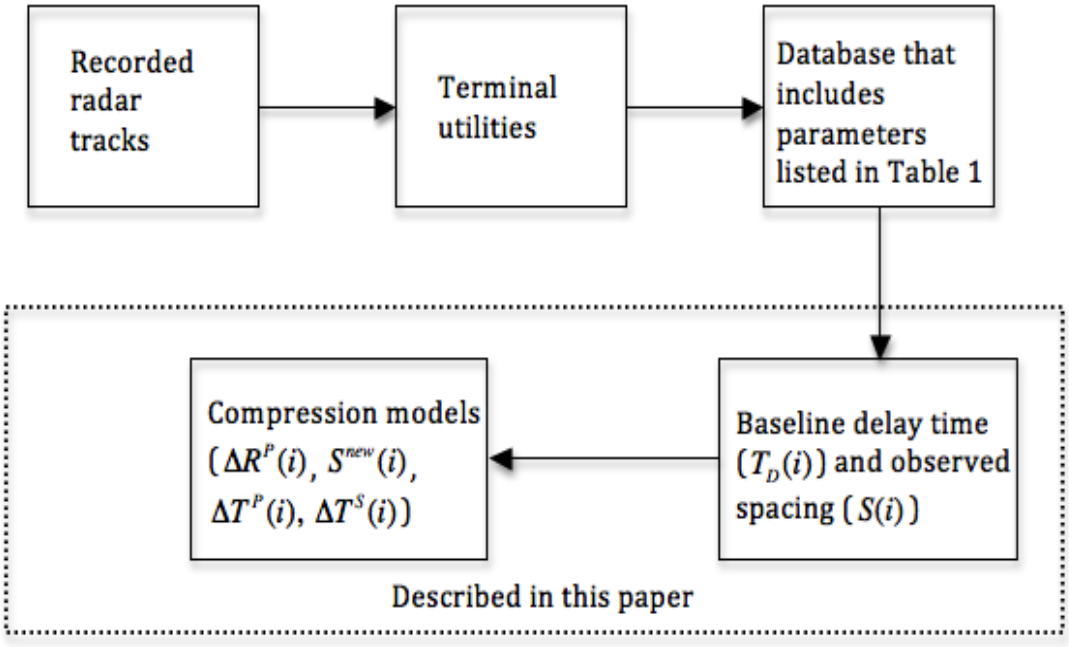

Figure 1. Compression Model Input Generation Flow Diagram.

Figure 1 depicts a top-level flow diagram of the generation of the input data used in the compression models. The mathematical notation used in the last two blocks in the flow diagram are defined in the nomenclature section and will be described in detail later. The procedure begins with the recorded flight plans and tracks of the Center/TRACON Automation System (CTAS).[12] A bundled set of post-processing scripts called Terminal Utilities performs various functions and calculations such as data integrity checks, required runway threshold separation, runway assignments, and determines various speeds and distances (e.g. ground, air, etc.). These calculations are described in more detail in Ref. 7. However, aircraft delay is not determined via the recorded radar tracks and subsequent Terminal Utilities post-processing because of prohibitively long execution times. In this paper, we estimate the aircraft delay as part of the compression models. It is not necessary that this delay estimate be precise because we are interested only in delay savings (i.e. relative delay values and not absolute).

Now, following the execution of the Terminal Utilities, a database of numerous aircraft parameters is generated. Included in this database are the X and Y coordinates of the aircraft. For the purpose this analysis, a 40 nmi radius from the applicable runway threshold defines the notional TRACON boundary. Figure 2 shows the TRACON entry and runway threshold coordinates for aircraft landing at KATL 27L.

The compression models make use of a subset of aircraft parameters captured upon entry into the TRACON and at the runway threshold (facilitated by the Terminal Utilities data processing—with the exception of meteorological conditions) and is listed in Table 1. The *entry* and *runway* subscribes correspond to parameters captured at the TRACON entry and runway threshold, respectively.

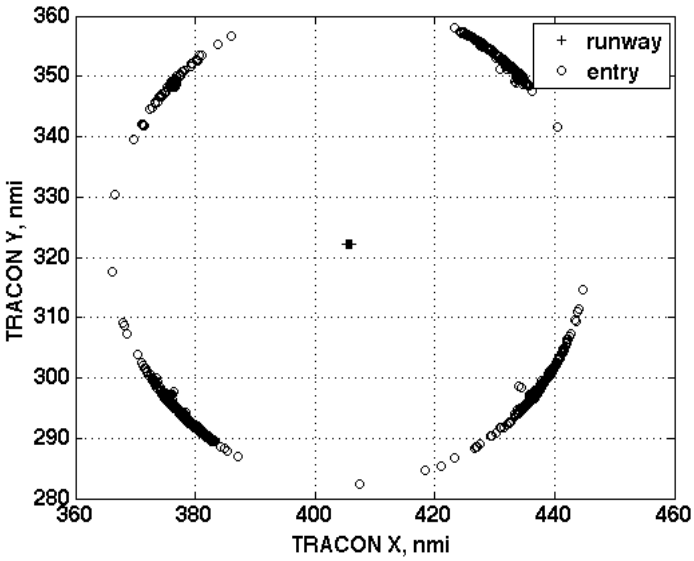

Figure 2. A80 TRACON Boundary Centered From KATL 27L.

The required spacing, S_R, is a function of the leading and trailing aircraft weight classes (commonly referred to as "3/4/5 spacing" to denote the required minimum separation in nmi).[13] The observed spacing, S, is the distance between the leading and trailing aircraft when the leading aircraft crosses the runway threshold. Path distance is the observed horizontal distance that the aircraft traverses. Ground distance is the estimated distance traveled by integrating the aircraft's observed ground speed with respect to time. Air distance is the estimated distance traveled by integrating the aircraft's estimated true airspeed (also with respect to time). Thus, the ground and air distances would be the same if there were no winds. Crossing times are captured at the TRACON entry, T_{entry}, and runway threshold, T_{runway}, in addition to the distances. Key flight attributes such as the aircraft identification (ID), arrival route (i.e., Standard Terminal Arrival Route (STAR)), and engine type (jet, turboprop, and piston) for each flight are also recorded. Airport meteorological conditions are retrieved from the FAA's Aviation System Performance Metrics (ASPM) quarter-hourly reports[14] and then fused into Table 1.

Table 1. Compression Model Input Data.

required longitudinal separation, S_R	ground distance at runway threshold, G_{runway}
observed longitudinal separation, S	entry ground distance, G_{entry}
path distance at runway threshold, P_{runway}	aircraft ID
entry path distance, P_{entry}	destination airport
runway threshold crossing time, T_{runway}	landing runway
TRACON entry time, T_{entry}	Standard Terminal Arrival Route (STAR)
air distance at runway threshold, A_{runway}	engine type (e.g. jet, turboprop)
entry air distance, A_{entry}	meteorological conditions (IMC or VMC)

The analysis uses the inputs provided in Table 1 to derive a reference delay time, $T_D(i)$ for each aircraft, i. This time establishes a reference time to facilitate relative delay savings calculations resulting from compressing the arrival traffic. The path distance flown for each aircraft, i, is calculated beginning with the first flight recorded on the first day of recordings (i=1) and ending with the last flight recorded on the last day of recordings,

$$R^P(i) = P_{runway}(i) - P_{entry}(i). \quad (1)$$

The air and ground distances are, respectively,

$$R^A(i) = A_{runway}(i) - A_{entry}(i) \tag{2}$$

and

$$R^G(i) = G_{runway}(i) - G_{entry}(i). \tag{3}$$

The transit time is

$$T(i) = T_{runway}(i) - T_{entry}(i). \tag{4}$$

The average true airspeed is determined using the air distance and transit time,

$$\bar{V}_{TAS}(i) = R^A(i) / T(i) \tag{5}$$

whereas the average ground speed uses of the ground distance and transit time,

$$\bar{V}_{GS}(i) = R^G(i) / T(i). \tag{6}$$

The average headwind for each aircraft is estimated as the difference between these average speeds:

$$\bar{V}_W(i) \approx \bar{V}_{GS}(i) - \bar{V}_{TAS}(i). \tag{7}$$

Arrival flights, for all days, are grouped by engine type, STAR, runway, and meteorological condition. This segregation results in a distribution of path distance, Eq. (1), and average true airspeed, Eq. (5) for each unique engine type/STAR/runway/meteorological condition grouping. Those aircraft that flew faster than the median are in a percentile greater than the 50th, but less than the 100th. Similarly, those aircraft that flew shorter distances than the median are in a percentile less than the 50th, but greater than the 0th. The strategic selection of a path distance and true airspeed percentile enables a delay time to be calculated. The extremes in the path distance and true airspeed distributions are avoided by limiting the minimum and maximum percentiles to the 10th percentile (path) and 90th percentile (speed). These outliers are included in the compression models, but do not receive any benefits. Hereafter, the minimum path distance that corresponds to a certain percentile is referred to as $R^P_{\min}(k)$ and the maximum (average) true airspeed that corresponds to a certain percentile is referred to as $\bar{V}^{\max}_{TAS}(k)$. The index k denotes that there are k unique engine type/STAR/runway/meteorological condition combinations. The minimum path distance for each aircraft, $R^P_{\min}(i)$, and maximum average true airspeed, $\bar{V}^{\max}_{TAS}(i)$, correspond to the appropriate $R^P_{\min}(k)$ and $\bar{V}^{\max}_{TAS}(k)$, respectively. The compression model does not allow path distances to increase. For those aircraft that have shorter than the statistically calculated minimum path distances (like the outliers mentioned above), the original path distance is used (i.e., if $R^P_{\min}(i) > R^P(i)$), then $R^P_{\min}(i) = R^P(i)$). A similar check on $\bar{V}^{\max}_{TAS}(i)$ is *not* performed. Now, a new ground speed for each aircraft is determined from the maximum true airspeed and average winds,

$$\bar{V}^{new}_{GS}(i) = \bar{V}^{\max}_{TAS}(i) + \bar{V}_W(i). \tag{8}$$

The ratio of the minimum path distance and this new ground speed establishes a minimum transit time,

$$T_{\min}(i) = R^P_{\min}(i) / \bar{V}^{new}_{GS}(i). \tag{9}$$

Finally, the reference delay time for each arriving flight is established as the observed transit time less the minimum transit time,

$$T_D(i) = T(i) - T_{\min}(i). \tag{10}$$

Delay time for each aircraft, $T_D(i)$, in conjunction with the observed spacing, S from Table 1, establish a reference for comparison and are hereafter referred to as the baseline. Two types of traffic compression models are used to quantify the potential reduction of excess spacing at the runway threshold and the corresponding delay savings. The first model is referred to as the path compression model because the flight's path distance can be reduced, but its observed average true airspeed is retained. The second model is referred to as the path and speed compression model because the flight's path distance can be reduced and its average true airspeed can be increased in order to recover additional excess spacing. Both traffic compression models result in new path distances flown, S^{new} (for comparison with S), and new reference delay times, T_D^{new} (for comparison with $T_D(i)$ provided in Eq. (10). The path compression model is described first, followed by the path and speed compression model.

A. Path Compression Model

The path compression model determines the excess spacing,

$$S_E(i) = S(i) - S_T(i), \tag{11}$$

which is the difference between the observed spacing and the target spacing, given below,

$$S_T(i) = S_R(i) + S_B(i), \tag{12}$$

where S_R is the required in-trail separation, and S_B is a spacing buffer. The spacing buffer is modeled as a normal random number with mean, μ, and standard deviation, σ,

$$S_B(i) \sim \mathrm{N}(\mu, \sigma). \tag{13}$$

The mean spacing buffer is set to 0.5 nmi. Its standard deviation is prescribed as half of the mean (σ = 0.25 nmi) based on the reasoning described in Ref. 1 indicating that 95% separation conformance is achieved within a buffer size at least twice that of the standard deviation. Eq. (13) models the in-trail spacing variations observed in actual operations. For each day of recorded aircraft traffic, Eqs. (14-16) determine the amount of path compression, the new path distance flown and the new excess spacing, respectively,

$$\Delta R^P(i) = R^P(i) - R^{new,P}(i), \tag{14}$$

$$R^{new,P}(i) = \begin{cases} \max\left\{R^P_{\min}(i), R^P(i) - \max(S_E(i), 0)\right\} & \text{if } i = 1 \\ \max\left\{R^P_{\min}(i), R^P(i) - \max(S_E(i) + \Delta R^P(i-1), 0)\right\} & \text{if } i > 1, \end{cases} \tag{15}$$

$$S_E^{new}(i) = \begin{cases} S_E(i) - \Delta R^P(i) & \text{if } i = 1 \\ S_E(i) - (\Delta R^P(i) - \Delta R^P(i-1)) & \text{if } i > 1. \end{cases} \tag{16}$$

The minimum value for $\Delta R^P(i)$ is zero occurring when $R^P_{\min}(i) = R^P(i)$. The new transit time after path compression is determined from the new path distance and original average ground speed

$$T^{new,P}(i) = R^{new,P}(i) / \bar{V}_{GS}(i). \tag{17}$$

The new runway threshold crossing time is

$$T_{runway}^{new,P}(i) = T_{runway}(i) - \Delta T^{P}(i), \tag{18}$$

where

$$\Delta T^{P}(i) = T(i) - T^{new,P}(i). \tag{19}$$

The new spacing and new delay time follow, respectively,

$$S^{new}(i) = S_R(i) + S_E^{new}(i), \tag{20}$$

$$T_D^{new}(i) = T_D(i) - \Delta T^{P}(i). \tag{21}$$

The delay savings resulting from path compression and excess spacing reduction is found using the baseline delay provided in Eq. (10) and the new delay time from Eq. (21),

$$\Delta T_D(i) = T_D(i) - T_D^{new}(i). \tag{22}$$

Because the metric of interest is a time change, Eq. (22) is equivalent to Eq. (19). That is, the reduced delay is naturally the reduced transit time. The new excess spacing calculated using Eq. (16) is never negative, ensuring that the original arrival sequence is preserved.

B. Path and Speed Compression

The path and speed compression model is an extension of the path compression model. The new transit time given in Eq. (17) above comes from flying a shorter path than the originally observed route while maintaining the same original average ground speed.

Modeling speed changes in addition to route changes is another compression strategy described next. Here, the minimum transit time is calculated using the new path distance, Eq. (15), and new average ground speed, Eq. (8),

$$T_{\min}^{*}(i) = R^{new,P}(i) / \bar{V}_{GS}^{new}(i). \tag{23}$$

Next, the two components of the time change are determined. The first component is the difference from the values found in Eq. (17) and Eq. (23),

$$\Delta T_1(i) = T^{new,P}(i) - T_{\min}^{*}(i). \tag{24}$$

The second component is the ratio of the new excess spacing (given in Eq. (16)) to the new ground speed,

$$\Delta T_2(i) = S_E^{new}(i) / \bar{V}_{GS}^{new}(i). \tag{25}$$

Estimating the time change as

$$\Delta T^{S}(i) = \min(\Delta T_1(i), \Delta T_2(i)), \tag{26}$$

where the superscript *S* indicates speed compression model. This enables the calculation of a new runway threshold crossing time, new transit time and new delay time given below in Eqs. (27-29), respectively,

$$T_{runway}^{new,S}(i) = T_{runway}^{new,P}(i) - \Delta T^{S}(i), \tag{27}$$

$$T^{new,S}(i) = T^{new,S}_{runway}(i) - T_{entry}(i), \tag{28}$$

$$T^{new,S}_{D}(i) = T_{D}(i) - (T_{runway}(i) - T^{new,S}_{runway}(i)). \tag{29}$$

Finally, the delay savings due to path and speed compression and excess spacing reduction is

$$\Delta T_{D}(i) = T_{D}(i) - T^{new,S}_{D}(i). \tag{30}$$

Algebraic manipulations (see Appendix) of Eqs. (18), (27), (29), and (30), reveal a more insightful expression for Eq. (30) showing that the delay savings is a linear combination of the delay savings of the path compression model, Eq. (19), and the speed compression model, Eq. (26),

$$\Delta T_{D}(i) = \Delta T^{P}(i) + \Delta T^{S}(i). \tag{31}$$

C. Scope

Results are shown for two busy runways in the United States. The two runways selected, KATL 27L and KDEN 35R, are chosen because they are independent runways dedicated to arrivals only. Zelinski identified several runway procedural constraints that could affect in-trail spacing in Ref. 1; the two runways chosen here are free from those constraints. Three types of results are shown: The sensitivity of the results to the compression model, the daily variation of the estimated delay savings and excess spacing reduction, and the excess spacing statistical distributions before and after path compression.

Sensitivity analyses are performed on the $R^{P}_{\min}$ and $\overline{V}^{\max}_{TAS}$ threshold percentiles in order to understand how they affect the estimated delay savings. As a reminder, these percentiles determine the reasonable "minimum" observed path distance and "maximum" average true airspeed, respectively. These percentiles are calculated on a per runway/STAR/engine type/meteorological condition basis. For the path compression model, the delay savings, Eq. (19), is unaffected by $\overline{V}^{\max}_{TAS}$, so two threshold percentiles are chosen for $R^{P}_{\min}$ to understand the range of ΔT_{D}. The chosen lower bound is the 50th percentile while the chosen upper bound is the 10th percentile. The path and speed compression model uses these same two $R^{P}_{\min}$ threshold percentiles in combination with two $\overline{V}^{\max}_{TAS}$ threshold percentiles (50th and 90th, the lower and upper limits of the true airspeed distribution, respectively). This results in a total of two discrete values of ΔT_{D} for the path compression model and four discrete values for the path and speed compression model.

The notation ${}_{10}R^{P}_{\min}$ indicates the minimum path distance value, $R^{P}_{\min}$, was assigned to the 10% percentile path distance value. Similar notation is used for the maximum average true airspeed, $\overline{V}^{\max}_{TAS}$. The two discrete values of ΔT_{D} for the path compression model correspond to ${}_{50}R^{P}_{\min}$ and ${}_{10}R^{P}_{\min}$. The four discrete values of ΔT_{D} for the path and speed compression model correspond to (1) ${}_{50}R^{P}_{\min}$, ${}_{50}\overline{V}^{\max}_{TAS}$, (2) ${}_{50}R^{P}_{\min}$, ${}_{90}\overline{V}^{\max}_{TAS}$, (3) ${}_{10}R^{P}_{\min}$, ${}_{50}\overline{V}^{\max}_{TAS}$, and (4) ${}_{10}R^{P}_{\min}$, ${}_{90}\overline{V}^{\max}_{TAS}$. This same notation will be retained in the results section below. Now, varying the percentile that defines the statistical minimum, $R^{P}_{\min}$, also affects the path distance saved, ΔR^{P}, given in Eq. (14) and will be shown in the results section.

Following the minimum path distance and maximum average true airspeed sensitivity analyses, the daily variations of delay savings, ΔT_{D}, and excess spacing reduction, ΔR^{P}, are examined for KATL 27L. The statistical minimum path distance is fixed at the 10th threshold percentile (${}_{10}R^{P}_{\min}$). Only results for the path compression model are presented.

Lastly, cumulative distribution functions (CDFs) are used to compare the baseline (i.e., observed) in-trail spacing and the in-trail spacing resulting from the path compression model for the 2.5 nmi required minimum separation. The analysis compares the percentage of flights with excess in-trail spacing of 0.5 nmi or less. In these analyses, the

delay time savings and path distance savings are provided in terms of the statistical median rather than the mean in order to lessen the affect of outliers in the data. The number of outliers is small (a fraction of a percent) and are the typical of data consistency errors encountered when analyzing large real air traffic data sets.

III. Results

A. Sensitivity of Results to $R^P_{\min}$ and $\bar{V}^{\max}_{TAS}$

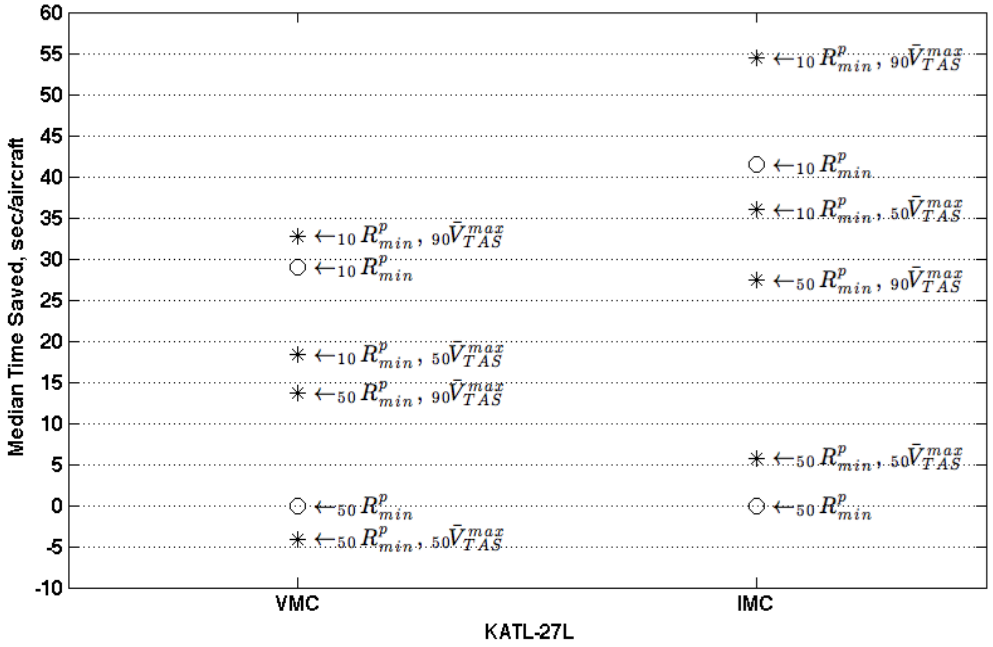

Figure 3. Median Delay Time Saved, ΔT_D, Per Flight In VMC And IMC at KATL 27L.

Figures 3 (above) and Fig. 4 (next page) show the effect of varying the "minimum" path distance and "maximum" average true airspeed threshold percentiles on the delay savings per flight at KATL 27L and KDEN 35R, respectively. Open circles denote the delay savings, Eq. (19), corresponding to the two $R^P_{\min}$ threshold values for the path compression model. Asterisks denote the delay savings, Eq. (31), corresponding to the four combinations of $R^P_{\min}$ and $\bar{V}^{\max}_{TAS}$ threshold percentiles for the path and speed compression model. For the path compression model, no delay savings are achieved when defining the minimum path distance as the median path distance ($_{50}R^P_{\min}$). With this definition, a significant number of aircraft were not allowed to lengthen their path, which would have resulted in negative delay savings. Although the average delay savings was not zero, this paper references the median as the statistical metric. Flying shorter than average routes in the terminal area, $_{10}R^P_{\min}$, reducing the excess spacing, compresses the arrival traffic and saves almost 30 seconds per flight for KATL 27L (Fig. 3) and nearly 60 seconds for KDEN 35R (Fig. 4) during VMC periods. During IMC periods, about 40 seconds are saved for KATL 27L (Fig. 3) and about 108 seconds for KDEN 35R (Fig. 4). The path and speed compression model achieves the most delay savings at the lower and upper bounds on the minimum path distance and maximum true airspeed percentiles, respectively ($_{10}R^P_{\min}$, $_{90}\bar{V}^{\max}_{TAS}$). In these circumstances, aircraft are flying faster on shorter routes (faster and shorter than the actual route/speeds flown).

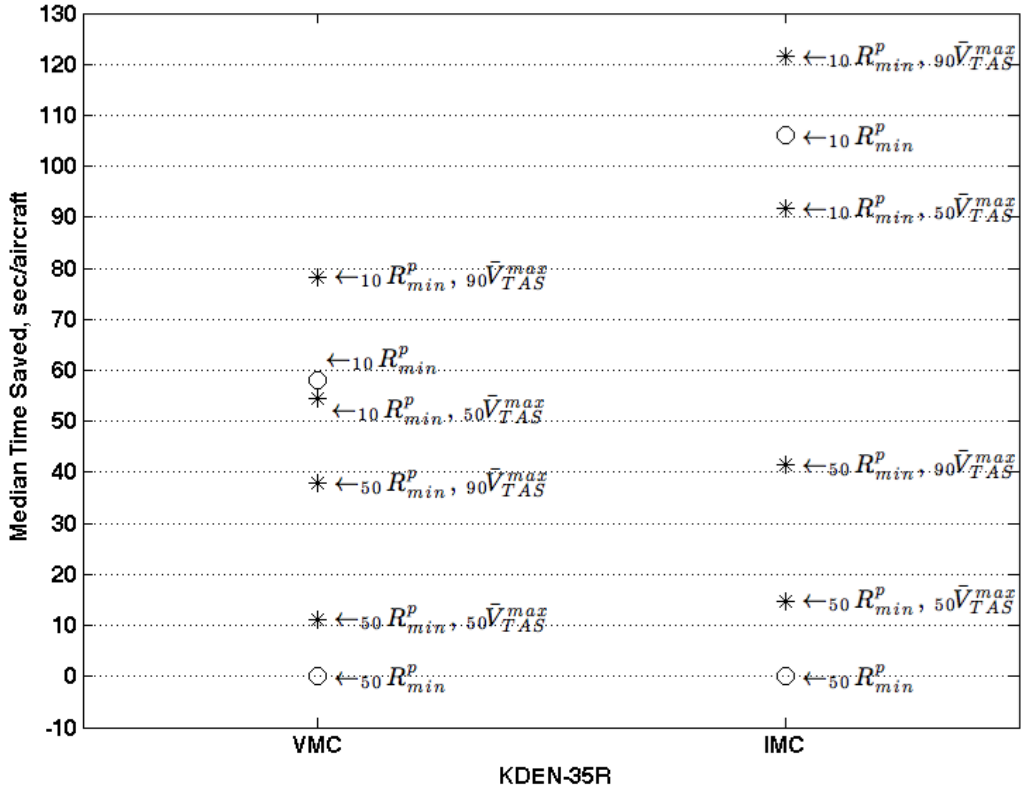

Figure 4. Median Delay Time Saved, ΔT_D, Per Flight In VMC And IMC at KDEN 35R.

A couple of trends can be observed in Fig. 3 and Fig. 4. First, there is greater delay savings during IMC periods than VMC periods, and greater savings at KDEN 35R than KATL 27L. These results are consistent with more excess in-trail spacing during IMC periods and at KDEN 35R. Second, there is greater sensitivity to the $R^P_{\min}$ threshold percentile than the $\bar{V}^{\max}_{TAS}$ threshold percentile. These results indicate that there is more variability in the path distances flown than the true airspeeds.

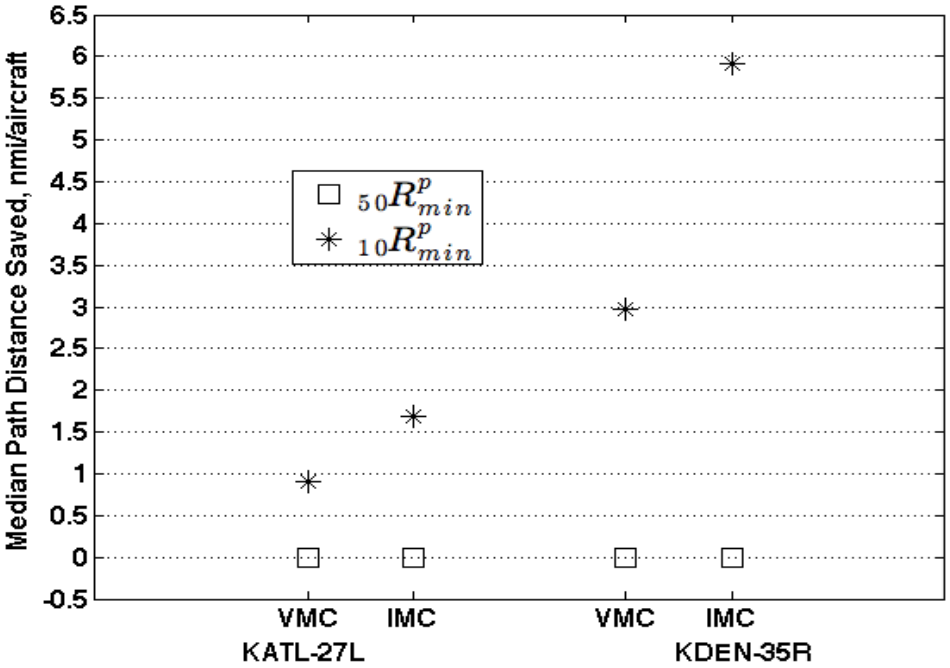

Figure 5. Median Path Distance Saved, ΔR , Per Flight In VMC And IMC.

Figure 5 shows the effect of varying the "minimum" path distance threshold percentile on the median path distance saved, Eq. (14). Speed compression does not reduce the path distance flown; thus, only $R^P_{\min}$ threshold percentiles are examined. Open squares indicate the 50th threshold percentile whereas asterisks indicate the 10th threshold percentile. Consistent with the delay savings shown in Fig. 3 and Fig. 4, path reductions are achieved when flying shorter than average routes, IMC reductions are greater than VMC, and are greater at KDEN 35R. In other words, there is more recoverable excess spacing in IMC than in VMC and more at KDEN 35R than KATL 27L.

B. Daily Variation of Results for KATL Runway 27L

The following three figures show data from analyses at KATL 27L. Figure 6 illustrates the daily variations of the delay savings, Fig. 7, the median path distance reduction, and Fig. 8, the number of flights during VMC and IMC periods. These analyses are presented for the path compression model with a fixed threshold value of ${}_{10}R^{P}_{\min}$.

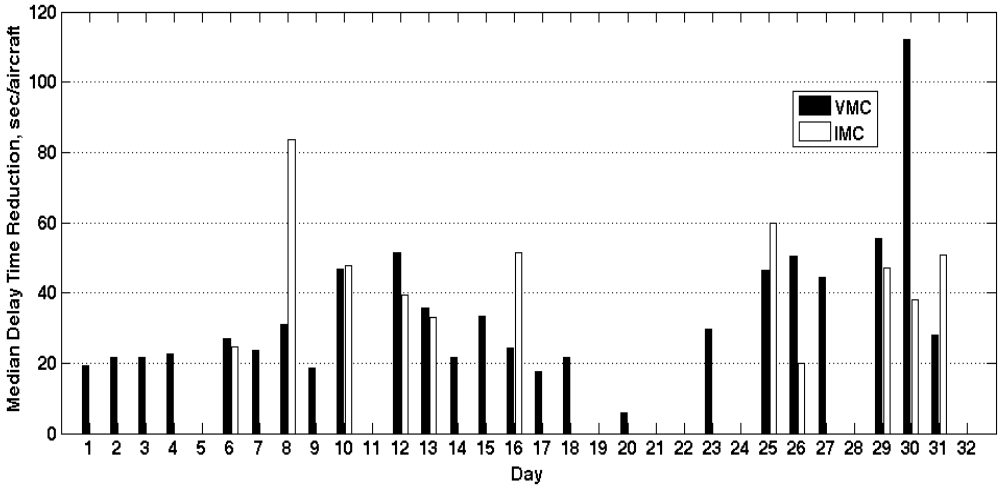

Figure 6. Median Daily Variation of Delay Time Saved at KATL 27L in IMC and VMC.

The delay savings shown in Fig. 6 varies from a few seconds per aircraft to roughly 115 seconds. Similar to the findings in Ref. 7, these results suggest that the day-to-day benefit pool of increased spacing precision will be quite variable.

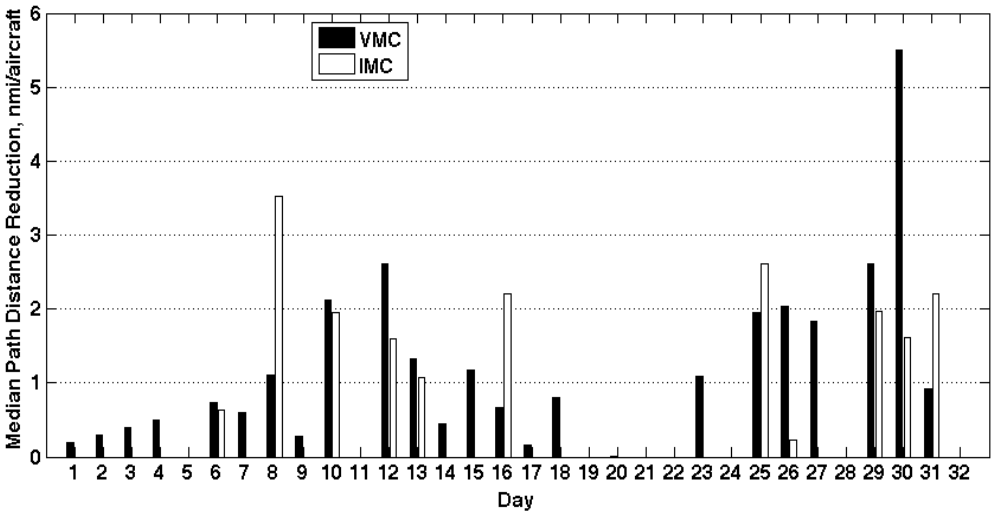

Figure 7. Median Daily Variation of Path Distance Saved at KATL 27L in IMC and VMC.

Similarly, Fig. 7 shows the daily variation of the path distance reduction. Values range from less than 1 nmi to about 5.5 nmi. Some of this daily variation is due to a low number of arrivals in the database for a given day – for example, the VMC results for Day 30. However, the cause(s) of much of the daily variation is not readily apparent. For example, Days 2, 3, 4, 15, and 27 each have about 500 flights and are exclusively VMC. Generally, these results are consistent with the findings reported in Ref. 7.

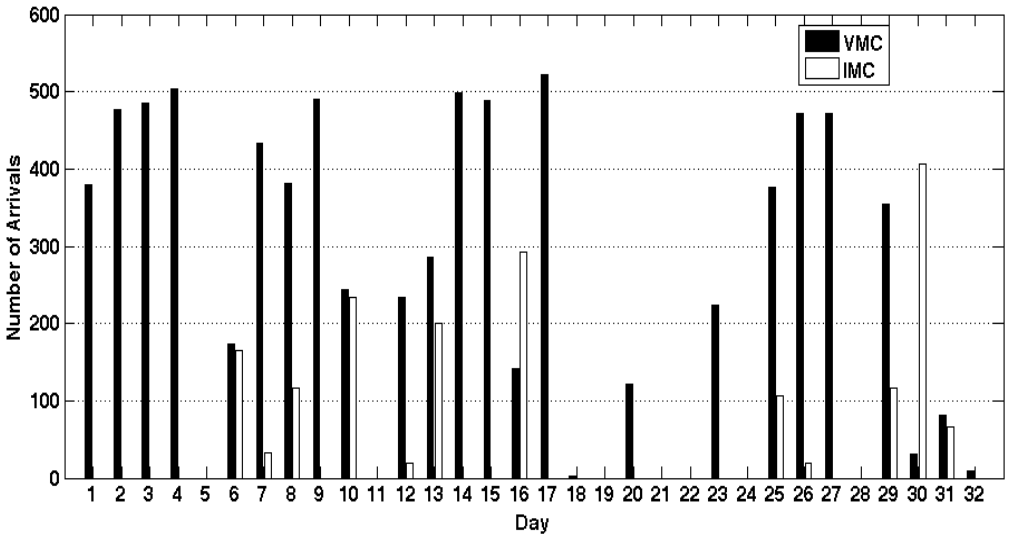

Figure 8. Daily Variation of Number of Arrivals at KATL 27L in IMC and VMC.

Most of the days that show no delay savings are a result of missing arrivals in the database for that day, as seen in Fig. 8. The missing flights were caused by a traffic recording malfunction that has since been resolved. Most of the days that show no delay savings are a result of missing arrivals in the database for that day, as seen in Fig. 8. Days 5, 11, 19, 21, 22, 24, and 28 did not have any tracks recorded. In addition, Days 18, 30, 31, and 32 have few VMC arrivals recorded, and Days 7, 12, 26, and 31 have few IMC arrivals recorded. Therefore, some of the results for these days can be particularly sensitive to the sample size. For example, the Day 8 IMC results and Day 30 VMC results should be considered outliers due to their low sample sizes relative to the other traffic days. The missing flights were caused by a traffic recording malfunction that has since been resolved.

C. Cumulative Distribution Functions

A cumulative distribution function (CDF) provides the probability of a random flight arriving with a leading/following aircraft wake vortex spacing less than or equal to x, where x is the spacing value of interest. This section provides the CDFs for (1) the observed in-trail spacing, S in Table 1 (referred to as the baseline) and (2) the in-trail spacing resulting from the path compression model, S^{new}, from Eq. (20). S and S^{new} are examined for those flights that require a minimum 2.5 nmi separation from the flight immediately ahead of it; most arrivals at KATL 27L and KDEN 35R are subject to that minimum required separation.

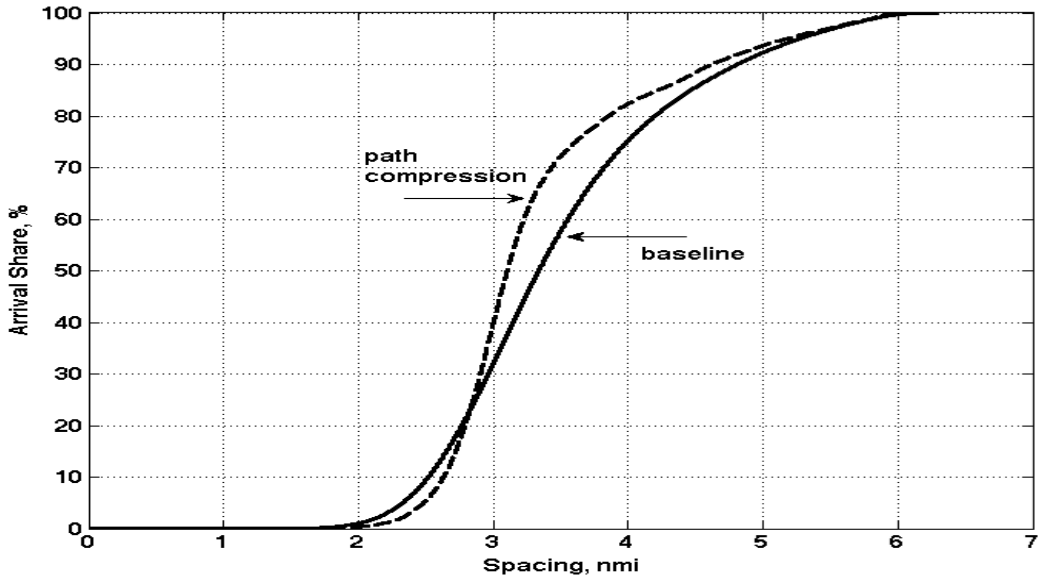

Figure 9. Cumulative Distribution Function, KATL 27L, VMC.

Figure 9 shows that as the in-trail spacing increases so do the likelihood of more flights achieving that spacing. Ten percent of the flights have less than the required minimum separation for the baseline (actual operations) whereas roughly 6% of the flights have less than the required minimum separation after adjustments are made with the path compression model. In these cases, the leading aircraft of the pair was compressed forward in time and more in-trail spacing was achieved. A crossover point exists at about 2.8 nmi after which the path compression model results in more arrivals with less excess spacing relative to the baseline. These results show that 20% (below crossover point) of flights are subjected to a slight increase of in-trail spacing while the remaining 80% (above crossover point) achieve a moderate reduction in excess spacing – roughly 0.25 nmi. Another suitable point of comparison is 3 nmi as this corresponds to the mean buffer of 0.5 nmi prescribed in Eq. (13). Thirty percent of flights land with a 3 nmi separation or less for the baseline whereas the path compression model increases the probability by 10% (40% of the arrivals achieving a spacing buffer of 0.5 nmi or less).

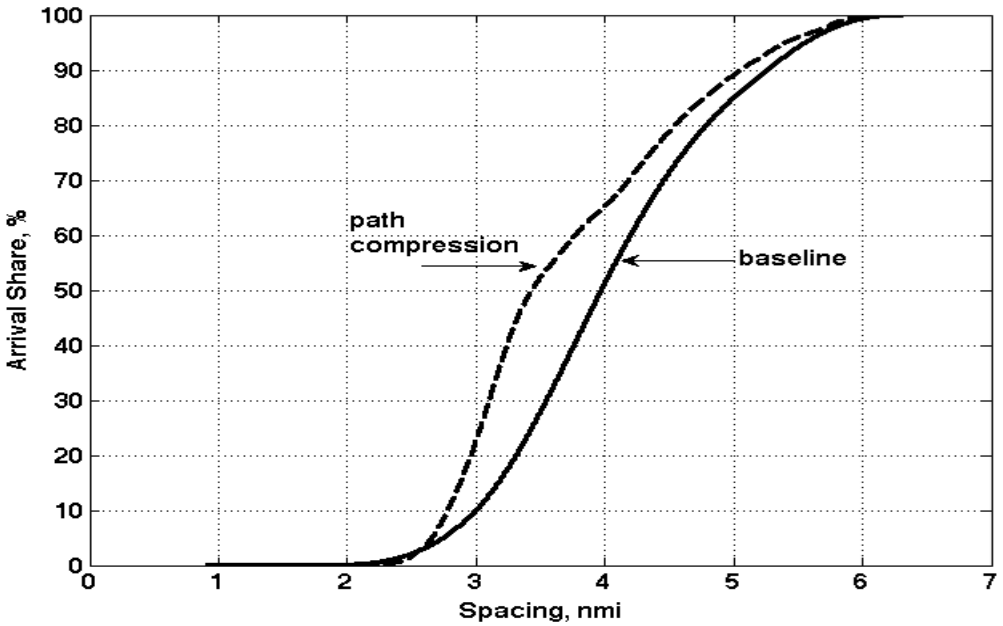

Figure 10. Cumulative Distribution Function, KATL 27L, IMC.

Figure 10 shows the CDFs for KATL 27L for aircraft operating in IMC periods; it is similar to the VMC CDFs in Fig. 9; however, there is no crossover point. For flights during IMC periods, there is a more substantial reduction in excess spacing that can be recovered – roughly 0.5 nmi. In other words, the observed excess in-trail separation present in the operations to KATL 27L is accompanied by enough corresponding excess path distance flown to allow its recovery.

The percentage of arrivals landing with excess spacing of 0.5 nmi (3 nmi spacing) or less is 10% for the baseline and 22% for the path compression model; an increase of 12%, roughly the same as the arrivals under VMC periods. However, more arrivals during IMC periods benefit (i.e., land with less excess spacing in general) as a result of the path compression than during VMC. This observation is made when comparing the area between the baseline and path compression CDFs in Fig 9 and Fig 10.

Now, after examining the CDFs for the 2.5 nmi reduced separation on final at KATL 27L, the CDFs for aircraft landing at KDEN 35R in VMC and IMC, are shown in Fig. 11 and Fig. 12, respectively.

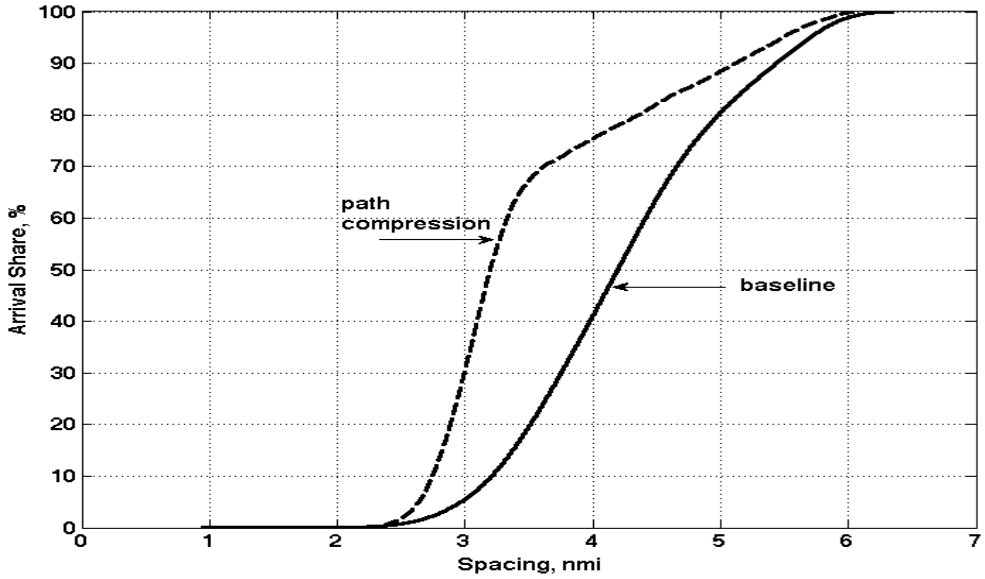

Figure 11. Cumulative Distribution Function, KDEN 35R, VMC.

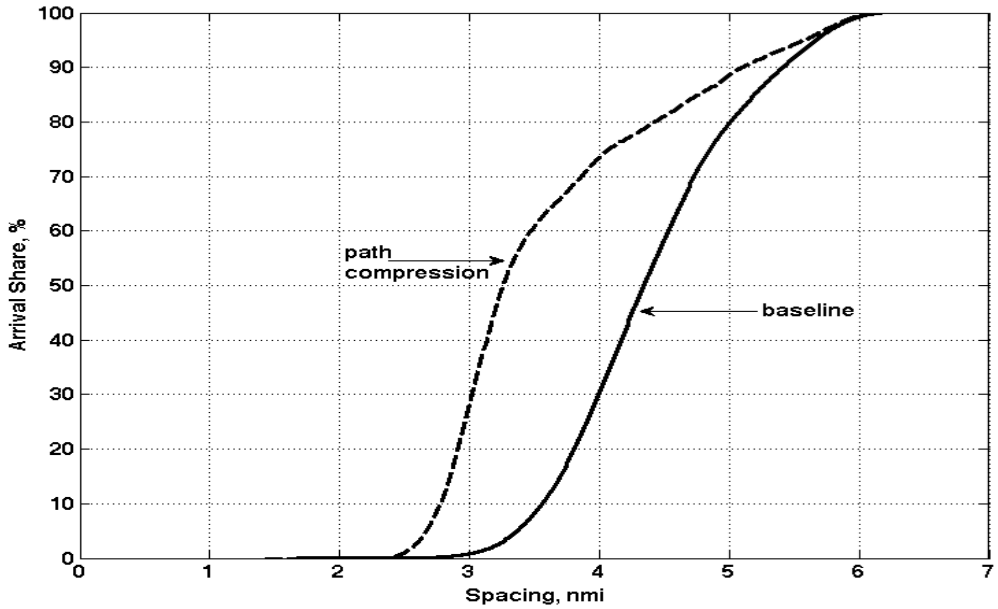

Figure 12. Cumulative Distribution Function, KDEN 35R, IMC.

Immediately apparent is the larger difference between the baseline and the path compression model relative to those shown for KATL 27L. Figure 11 (previous page) shows that ~5% of the baseline arrivals land with 3 nmi spacing (excess separation of 0.5 nmi). The path compression model achieves ~30%, a 25% increase over actual operations. Figure 12 presents the last CDF in this analysis for arrivals during IMC periods. Very few baseline arrivals, about 2%, land with excess spacing of 0.5 nmi compared to ~30% resulting from the path compression.

IV. Conclusion

A statistical modeling method for accessing the potential benefits of terminal scheduling and spacing automation tools has been developed and described. The key to such a statistical model is a sufficiently large data set of recorded flights. The model is referred to as a traffic compression model because it estimates delay reduction when excess spacing is recovered by shortening each aircraft's path and (optionally) increasing its speed closer to its shortest and fastest reasonable limits, respectively. This model does not require the trajectory reconstruction/generation procedure of modeling RNAV routes. Instead, our compression models can quickly provide first order analysis of potential delay savings achieved by reducing excess leading/following aircraft wake vortex separation using aircraft parameters captured at just two discrete locations in the trajectory: TRACON entry and runway threshold crossing.

Thousands of arrivals recorded over a five-month period in early 2010 enabled an analysis of observed wake vortex separation at KATL 27L and KDEN 35R (referred to as the baseline). A path compression model and its variant that models faster average airspeeds in the terminal area are utilized to examine the potential delay savings. Keys to the models are path and true airspeed distributions for aircraft flying on the same STAR to the same runway with the same engine type and operating in the same meteorological conditions. Selecting a percentile within the path and speed distribution produces two important parameters, the minimum path distance ($R^P_{\min}$), and the maximum average true airspeed ($\overline{V}^{\max}_{TAS}$), respectively. Varying $R^P_{\min}$ and $\overline{V}^{\max}_{TAS}$ results in a range of potential delay savings.

From the results of the $R^P_{\min}$ and $\overline{V}^{\max}_{TAS}$ sensitivity analysis (both path and path with speed compression models), we conclude the following:

- Delay savings are more sensitive to $R^P_{\min}$ than $\overline{V}^{\max}_{TAS}$
- More potential savings exist at KDEN 35R than KATL 27L
- More potential savings in IMC than VMC

- At KATL 27L, median delay savings per flight varied from -5 to 33 seconds in VMC and 0 to 55 seconds in IMC
- At KDEN 35R, median delay savings per flight varied from 0 to 80 seconds in VMC and 0 to 120 seconds in IMC

Following the sensitivity analysis, the daily variations of delay and path savings were examined with the path compression model using ${}_{10}R^{P}_{\min}$. The reduction in excess spacing was also examined for those arrivals that required a 2.5 nmi separation using CDFs. This second half of the analysis found:

- Uneven daily delay and path savings
- At KATL 27L, 10% increase over the baseline in arrivals landing with an excess spacing of 0.5 nmi or less and 25% increase at KDEN 35R

This study found that potential benefits of scheduling and spacing automation tools can be estimated by a statistical traffic compression model that makes use of aircraft parameters captured at just two descrete trajectory locations. This method eliminates the need to reconstruct and examine the entire trajectory from the TRACON meter fix to the runway threshold for each aircraft. And, it can be used irrespective of how the excess leading/following aircraft wake-vortex separation is reduced.

Appendix

Substituting Eq. (18) into Eq. (27) yields

$$T^{new,S}_{runway}(i) = T_{runway}(i) - \Delta T^{P}(i) - \Delta T^{S}(i). \tag{A1}$$

Now, substitute Eq. (A1) into Eq. (29),

$$T^{new,S}_{D}(i) = T_{D}(i) - \Delta T^{P}(i) - \Delta T^{S}(i). \tag{A2}$$

Finally, substituting Eq. (A2) into Eq. (30),

$$\Delta T_{D}(i) = \Delta T^{P}(i) + \Delta T^{S}(i), \tag{A3}$$

produces the expression given in Eq. (31).

References

[1]Zelinski, S., "Benefits of Precision Scheduling and Spacing for Arrival Operations," *31st Digital Avionics Systems Conference*, Williamsburg, Virginia, October 14-18, 2012.

[2]Federal Aviation Administration, Aerospace Forecast Fiscal Years 2012-2032 URL: www.faa.gov/about/office_org/headquarters_offices/apl/aviation_forecasts/aerospace_forecasts/2012-2032 [cited 1 November 2012].

[3]Joint Planning and Development Office, "Concept of Operations for the Next Generation Air Transportation System," Version 2.0, June 2007.

[4]Thipphavong, J., Mulfinger, D., "Design Considerations for a New Terminal Area Arrival Scheduler," *10th AIAA Aviation Technology Integration and Operations Conference*, Ft. Worth, Texas, September 13-15, 2012.

[5]Swenson, H. N., et al., "Design and Evaluation of the Terminal Precision Scheduling and Spacing System," *9th USA/Europe Air Traffic Management Research and Development Seminar*, Berlin, Germany, June 14-17, 2011.

[6]Thipphavong, J., et al., "Evaluation of the Controller-Managed Spacing Tools, Flight-deck Interval Management and Terminal Area Metering Capabilities for the ATM Technology Demonstration #1," *10th USA/Europe Air Traffic Management Research and Development Seminar*, Chicago, Illinois, June 10-13, 2013.

[7]Robinson III, J. E. and Kamgarpour, M., "Benefits of Continuous Descent Operations in High-Density Terminal Airspace Under Scheduling Constraints," *10th AIAA Aviation Technology Integration and Operations Conference*, Fort Worth, Texas, September 13-15, 2010.

[8]Yoon, Y. and Hansen, M., "The Impact of Advanced Technology on Next Generation Air Transportation: A Case Study of Required Navigation Performance (RNP)," AIAA-2007-6697, *AIAA Modeling and Simulation Technologies Conference and Exhibit*, Hilton Head, South Carolina, August 20-23, 2007.

[9]Zelinski, S., "A Graph-Based Approach to Defining Nominal Terminal Routing," *31st Digital Avionics Systems Conference*, Williamsburg, Virginia, October 14-18, 2012.

[10]Federal Aviation Administration, "Standard Operating Procedures", Order A80 7110.65E CHG2, February 25, 2013 URL: http://www.faa.gov [cited 1 February 2013].

[11]Federal Aviation Administration, "Control Positions of Operation and Standard Operating Procedures (SOP)", Order D01 7110.1H, April 12, 2012 URL: http://www.faa.gov [cited 1 February 2013].

[12]Swenson, H. N., et al., "Design and Operational Evaluation of the Traffic Management Advisor at the Fort Worth Air Route Traffic Control Center," *1st USA/Europe Air Traffic Management Research & Development Seminar*, Sarclay, France, June 16-19, 1997.

[13]Federal Aviation Administration, "Air Traffic Organization Control", Order JO 7110.65U CHG 2, March 7, 2013 URL: http://www.faa.gov [cited 1 February 2013].

[14]Federal Aviation Administration, 2011-2015 National Plan of Integrated Airport Systems Report, URL: http://aspm.faa.gov [cited 28 October 2012].